Characterization of Selectively ^{13}C-Labeled Synthetic Melittin and Melittin Analogues in Isotropic Solvents by Circular Dichroism, Fluorescence, and NMR Spectroscopy†

Arthur J. Weaver,‡ Marvin D. Kemple,*,§ and Franklyn G. Prendergast*,‡

Department of Biochemistry and Molecular Biology, Mayo Foundation, Rochester, Minnesota 55905, and Department of Physics, Indiana University-Purdue University at Indianapolis, Indianapolis, Indiana 46205-2810

Received March 6, 1989; Revised Manuscript Received June 9, 1989

ABSTRACT: The spectroscopic and functional characterization of ^{13}C-labeled synthetic melittin and three analogues is described. Selectively ^{13}C-enriched tryptophan ([$^{13}C\delta_1$]-L-Trp) and glycine ([$^{13}C\alpha$]Gly) were incorporated into melittin and three analogues by de novo peptide synthesis. ^{13}C-Labeled tryptophan was incorporated into melittin at position 19 and into single-tryptophan analogues of melittin at positions 17, 11, and 9, respectively. Each of the synthetic peptides contained ^{13}C-labeled glycine at position 12 only. The peptides were characterized functionally in a cytolytic assay, and spectroscopically by CD, fluorescence, and NMR. The behavior of ^{13}C-labeled synthetic melittin was, in all respects, indistinguishable from that of the naturally occurring peptide. All of the analogues were found to be efficient lytic agents and thus were functionally similar to the native peptide, yet no evidence was found for formation of a melittin-like tetramer by any of the analogues in aqueous media, although there was a propensity for apparently nonspecific peptide aggregation, especially for MLT-W9. Since the analogues did exhibit fractional helicities by CD comparable to or even greater than melittin itself in the presence of methanol, we infer that tetramer assembly requires not only the ability to form α-helix but also a very precise packing of amino acid side chains of the constituent monomers. The ^{13}C chemical shift of the Gly-12 Cα was found to be a sensitive marker for helix formation in all of the peptides. For melittin itself, ^{13}C NMR spectra revealed a downfield shift of $\sim$1.8 ppm for the Gly-12 $^{13}C\alpha$ resonance of the tetramer relative to that observed for the free monomer in D_2O. In mixed samples containing melittin monomer and tetramer, two discrete Gly-12 $^{13}C\alpha$ peaks were observed simultaneously, suggestive of slow exchange between the two species. We conclude that melittin's ability to form a soluble tetramer is not a prerequisite for cytolytic activity, nor is cytolytic potential precisely correlated with the ability to form an amphiphilic helix.

Melittin is an intensively studied cytolytic peptide which is known to exist in different structural forms depending on sample conditions. This peptide is an excellent choice as a model for the assembly of a soluble protein oligomer in that it lacks organized or stable secondary structure at submillmolar concentrations in pure water yet becomes predominantly helical and tetrameric in media of high ionic strength or high pH (Talbot et al., 1979). Further, the crystal structure of tetrameric melittin has been solved to 2-Å resolution (Terwilliger & Eisenberg, 1982a,b). In addition, melittin also presents a useful model for the study of peptide–lipid interactions since it interacts avidly with lipid surfaces, which is apparently a major factor in its ability to lyse lipid vesicles and cells (Sessa et al., 1969; Schröder et al., 1971; Knöppel et al., 1979). Elucidation of the molecular determinants of assembly of the soluble tetramer and of the cytolytic activity of melittin would thus be of considerable value in enhancing understanding of structure–function relationships in peptides and proteins. The relatively simple structure of melittin and its ready direct synthesis make it possible to devise strategies using heteronuclear NMR of isotopically labeled melittin to probe structure–function correlations. One such study of hydrophobic oligopeptides labeled with ^{13}C-enriched Trp has been reported (Weaver et al., 1988).

In this work, the synthesis and characterization of selectively ^{13}C-enriched melittin is described. In addition, three analogues of melittin were synthesized in which the position of the single Trp residue was changed. In each case, the synthetically incorporated Trp was selectively labeled with ^{13}C at the Cδ_1 position (i.e., the 2-position) of the indole ring (Branchini et al., 1987). The objective was to use both fluorescence and ^{13}C NMR signals from the [$^{13}C\delta_1$]Trp side chain to probe the environment and mobility of the indole moiety in the respective analogues. [$^{13}C\alpha$]Glycine was also incorporated into each of the synthetic peptides at position 12 to serve as an NMR marker for the environment and motion of the peptide backbone. Aside from the obvious benefits of site-specific ^{13}C labeling in NMR studies of these peptides, the use of synthetic melittin avoids the problem of phospholipase A_2 contamination in studies of melittin–lipid interactions and ensures peptide homogeneity (cf. formylated and nonformylated natural melittin). In this work, the general properties of ^{13}C-labeled synthetic melittin and analogues in isotropic solvents were characterized by using a variety of techniques including NMR, fluorescence, and CD spectroscopies and HPLC[1] gel filtration.

† This work was supported by Grant NI486K0521 from the Office of Naval Research. The NT-300 NMR spectrometer at IUPUI was purchased with partial support from the National Science Foundation (PCM 8018725). K^{13}CN used in the synthesis of [$^{13}C\delta_1$]-L-tryptophan was provided in part by the Los Alamos Stable Isotope Resource, which is supported by the National Institutes of Health (RR02231) and the U.S. Department of Energy/Office of Health and Environmental Research Stable Isotope Program.

* Address correspondence to these authors.

‡ Mayo Foundation.

§ Indiana University–Purdue University at Indianapolis (IUPUI).

0006-2960/89/0428-8614$01.50/0

MLT-
W19 G I G A V L K V L T T G* L P A L I S W* I K R K R Q Q
W17 G I G A V L K V L T T G* L P A L W* S L I K R K R Q Q
W11 G I G A V L K V L T W* G* L P A L I S L I K R K R Q Q
W9 G I G A V L K V W* T T G* L P A L I S L I K R K R Q Q
5 10 15 20 25

FIGURE 1: Amino acid sequences of melittin (MLT-W19), MLT-W17, MLT-W11, and MLT-W9. The single Trp residue is shown in bold type to emphasize its location in the respective analogues. The Leu-19 residue is also shown in bold type to indicate that the primary sequence of the analogue differs from that of melittin at this position as well. ^{13}C-Labeled residues are started. All of the synthetic peptides are amidated at the C-terminus.

The relative cytolytic potency of the peptides was assessed by using a simple light transmittance assay.

The following questions were posed: Do the analogues retain cytolytic activity? Does the location of the Trp residue along the melittin amphiphilic helix influence oligomer formation? Can specific structural elements be correlated with membranolytic action or tetramer formation?

Materials and Methods

Peptide Synthesis. Melittin and three analogues were synthesized de novo by solid-phase techniques. The primary sequences of the synthetic peptides are given in Figure 1. The peptides were named according to the position of the single Trp residue; synthetic melittin was designated MLT-W19, while analogues with the Trp residue at position 17, 11, or 9 were designated MLT-W17, MLT-W11, and MLT-W9, respectively.[2] In each of the analogues, leucine was substituted at position 19 for the displaced Trp. Amino acid analysis, peptide sequencing, and mass spectrometry were used to verify peptide homogeneity, sequence integrity, molecular weight, and isotope incorporation into the purified peptides.

Successful synthesis of MLT-W19 and analogues depended most critically on measures taken to optimize the yield of every synthetic step. Three modifications of the standard automated coupling procedure were adopted: (a) repetition of the coupling reaction between the incoming *t*-Boc-amino acyl anhydride and the deprotected peptidyl-resin; (b) maintenance of adequate solvent volumes and reagent quantities to assure suspension and complete reaction of the entire resin volume, which was often found to expand disproportionately with peptide length; and (c) the inclusion of manual synthetic steps to incorporate the ^{13}C-labeled amino acids into the peptide sequences, thereby avoiding losses associated with the automated symmetric anhydride coupling strategy.

For each of the peptides, 0.5 mmol of *p*-methylbenzhydrylamine (MBHA) resin was used as the solid-phase support. HF cleavage of the peptidyl-MBHA resins yielded C-terminal amidated peptides as are found in naturally occurring melittin. All automated steps were performed on an Applied Biosystems 430A peptide synthesizer using reagents of the highest grade commercially available. 2-^{13}C-Labeled indole was prepared as described by Branchini et al. (1987). [$^{13}C\delta_1$]-L-Tryptophan[3] was prepared by an enzymatic method from the labeled indole by Cambridge Isotope Laboratories (Woburn, MA) and incorporated into the synthetic peptides after chemical protection of the primary amino group with di-*tert*-butyrl dicarbonate according to a procedure adapted from Moroder et al. (1976). [$^{13}C\alpha$]Glycine was purchased from the same source and protected in a similar fashion.

Prior to manual coupling of the ^{13}C-labeled residues, the peptidyl resin was deprotected with trifluoroacetic acid (TFA) on the automated synthesizer. The resin was transferred to a large (~50-mL) manual reaction vessel, neutralized in 25 mL of 12.5% diisopropylethylamine (DIEA) in CH_2Cl_2 for 10 min, and then washed with 3 × 20 mL of CH_2Cl_2. The aminoacyl to peptidyl-resin coupling reaction was carried out in 1:1 *t*-Boc-amino acid/dicyclohexylcarbodiimide (DCC) to minimize the amount of ^{13}C-labeled amino acid used. Typically, a 1.1–1.5-mequiv excess of *t*-Boc-[^{13}C]amino acid to peptidyl-resin was used to achieve a ninhydrin-negative result (>98% coupling yield).

In the synthesis of MLT-W11, *t*-Boc-[$^{13}C\alpha$]Gly and *t*-Boc-[$^{13}C\delta_1$]-L-Trp were added by manual steps at position 12 and position 11, respectively. Undiluted TFA containing indole (4 mg/mL) and anisole (4 μL/mL) was used for deprotection of the *t*-Boc-[$^{13}C\alpha$]-L-Gly-peptidyl-MBHA resin prior to manual addition of the *t*-Boc-[$^{13}C\delta_1$]Trp residue; the procedure was otherwise as described above. The resulting 16 amino acid *t*-Boc-peptidyl-resin was then transferred back to the automated synthesis reaction vessel and the MLT-W11 sequence completed. The other synthetic peptides each required an additional transfer for addition of their discontiguous ^{13}C-labeled residues. After the final *t*-Boc-glycyl residue was attached to the peptidyl-MBHA resin, the N-terminal *t*-Boc protecting group was removed in an automated step. The completed resin was washed repeatedly in CH_2Cl_2 and then in 1:1 CH_3OH/CH_2Cl_2, and dried overnight over a vacuum. Standard procedures were employed for final HF cleavage of the crude peptides from the MBHA resin.

Each of the synthetic peptides was protected from exposure to light throughout synthesis and during subsequent manipulations to avoid possible photodegradation. Peptide concentrations were determined by measuring the ultraviolet absorption at 280 nm, assuming a molar extinction coefficient of 5570 M^{-1} cm^{-1} (Quay & Condie, 1983). The crude yields of the cleaved synthetic peptides were 400–500 mg (28–35% of theoretical yield).

Peptide Purification. The purity of the crude cleaved peptides, as determined by analytical reversed-phase (RP) HPLC was sufficiently high to allow purification of 50–100 mg of peptide per injection by direct application of a concentrated solution onto a semipreparative column (Vydac C18-300, 250 × 4.6 mm; Separations Group, Hesparia, CA) running a CH_3CN/H_2O solvent gradient. To ensure minimal contamination of the final product, only the central fractions of the largest peak absorbing at 280 nm were collected in each semipreparative run. By this method, the total purified yields were 100–150 mg (7–11% of theoretical yield) for each of the synthetic peptides.

[1] Abbreviations: Bis-Tris, [bis(2-hydroxyethyl)amino]tris(hydroxymethyl)methane; DCC, dicyclohexylcarbodiimide; DIEA, diisopropylethylamine; DMF, dimethylformamide; DMSO-d_6, dimethyl-d_6 sulfoxide; DSS, sodium 2,2-dimethyl-2-silapentanesulfonate; EDTA, ethylenediaminetetraacetic acid; FABMS, fast atom bombardment mass spectrometry; HPLC, high-pressure liquid chromatography; MBHA, *p*-methylbenzhydrylamine; MLT-W19, [[$^{13}C\delta_1$]-L-Trp-19,[$^{13}C\alpha$]Gly-12]-melittin; MLT-W17, [[$^{13}C\delta_1$]-L-Trp-17,[$^{13}C\alpha$]Gly-12,Leu-19]melittin; MLT-W11, [[$^{13}C\delta_1$]-L-Trp-11,[$^{13}C\alpha$]Gly-12,Leu-19]melittin; MLT-W9, [[$^{13}C\delta_1$]-L-Trp-9,[$^{13}C\alpha$]Gly-12,Leu-19]melittin; PDMS, plasma desorption mass spectrometry; RP-HPLC, reversed-phase high-pressure liquid chromatography; SDS–PAGE, sodium dodecyl sulfate–polyacrylamide gel electrophoresis; TBME, *tert*-butyl methyl ether; *t*-Boc, *tert*-butyloxycarbonyl; TFA, trifluoroacetic acid; Tris, tris(hydroxymethyl)-aminomethane.

[2] The ^{13}C-labeled synthetic peptides described in this work are hereafter referred to only by their designated MLT-W names to avoid confusion with naturally occurring melittin.

[3] "[$^{13}C\delta_1$]-L-Tryptophan" denotes tryptophan labeled at the 2-position with ^{13}C.

Methods used to assess the homogeneity of the purified synthetic peptides included (a) amino acid analysis (Waters Instruments Picotag workstation for amino acid derivatization in line with Beckman 114M HPLC pumps and a Beckman 450 data system), (b) amino acid sequencing (Applied Biosystems 470A gas-phase sequenator), (c) sodium dodecyl sulfate–polyacrylamide gel electrophoresis (SDS–PAGE) using 22% gels, (d) plasma desorption mass spectrometry (PDMS) (BIO-ION Nordic BIN-10K plasma desorption mass spectrometer), and (e) fast atom bombardment mass spectroscopy (FABMS) (VG 30-250 quadrupole mass spectrometer).

Amino acid analysis and sequencing of each peptide yielded the appropriate amino acid composition and correct sequence for the purified product. SDS–PAGE showed that the synthetic species comigrated with naturally occurring melittin and did not show contaminants on overload gels.

Mass spectrometric analysis of the peptides provided the most sensitive assessment of homogeneity and chemical integrity of the purified ^{13}C-labeled synthetic peptides. For PDMS, the peptide samples ($\sim$3 nmol) were applied to nitrocellulose-coated aluminum foils as a 1:1 (mol/mol) solution in glutathione and then rapidly dried by centrifugation. Within the accuracy of the instrument, PDMS spectra of the respective synthetic peptides showed sharp peaks corresponding to the predicted position of the peptide molecular ion at the appropriate molecular mass (data not shown). For FABMS, the peptides were prepared in a matrix of 5:1 dithiothreitol/dithioerythritol heated at 90 °C to produce a homogeneous viscous liquid and then subjected to mass spectrometry. Results of the FABMS analysis showed excellent agreement of predicted with observed masses for the synthetic peptides (predicted mass values are given in parentheses): *Apis mellifera* melittin, 2845.9 (2845.76); MLT-W19, 2847.8 (2847.77); MLT-W11, 2859.7 (2859.81); MLT-W9, 2848.0 (2847.77). In all cases, the uncertainty in experimental mass values was ±0.1. Mass spectrometric analysis of MLT-W17 was not performed.

Cytolytic Assay. A simple spectrophotometric assay was designed to assess the relative cytolytic potency of MLT-W19 and analogues by measuring the kinetics of peptide-induced lysis of human erythrocytes.

Two 5-mL aliquots of human blood drawn into EDTA-containing tubes were centrifuged at 2600 rpm for 15 min followed by removal of the serum and resuspension of the erythrocytes in isotonic sucrose–phosphate buffer (0.3 M sucrose, 0.01 M sodium phosphate, pH 7.30). The erythrocytes were centrifuged (2600 rpm, 10 min) and resuspended in fresh buffer three additional times. Washed cells were exposed to equal amounts of each peptide, and the extent of hemolysis was assayed by measuring the transmittance of 650-nm light through the erythrocyte suspensions. The viscosity of the sucrose solution prevented sedimentation of cells over the time course of a given experiment. The assay was performed three times for each of the synthetic peptides under identical conditions by rapidly adding 0.2 nmol of peptide to 1.00 mL of an erythrocyte suspension which had been adjusted to an A_{650} of 1.0 in the absence of added peptide. After three inversions of the absorbance cuvette to effect mixing, the A_{650} was then followed from t = 20 s to $t \approx 10$ min.

All absorbance measurements were performed on a Cary 219 spectrophotometer equipped with an analog to digital converter and interfaced with an IBM AT personal computer. Kinetic data were processed with software developed by On-Line Instrument Systems (Jefferson, GA). Measurements of the time-dependent decrease in optical density at 650 nm due to peptide-induced hemolysis of erythrocytes were consistently reproducible with minimal variability ($\Delta A \leq 0.05A_{650}$). Control experiments with solutions of completely lysed cells showed that no absorbance due to hemoglobin or other released cellular constituents was detectable at 650 nm. The time-dependent decrease in A_{650} upon incubation of an erythrocyte suspension with peptide thus measured the decreasing number of intact erythrocytes that would otherwise scatter 650-nm light.

Gel Filtration. Gel filtration of the purified synthetic peptides was performed on a Beckman Spherogel TSK SW-2000 size-exclusion column run isocratically in low-salt (0.1 M NaCl, 10 mM Bis-Tris, pH 6.0) or high-salt (1.2 M NaCl, 10 mM Bis-Tris, pH 6.0) buffer at a flow rate of 0.8 mL min^{-1}. Samples were applied to the column in 50 μL of the appropriate buffered solution at a peptide concentration of 100 μM. Selected protein and small molecule standards of known molecular weight were also run under the same (nondenaturing) conditions and are given here in order of decreasing molecular weight: human hemoglobin (68 000); human serum albumin (66 000); hen egg white lysozyme (14 200); horse heart cytochrome *c* (12 400); and riboflavin (376.4). Reproducibility of the observed retention times for the synthetic peptides and standards was excellent (±0.1 min) in both low- and high-salt solutions.

CD Spectroscopy. CD spectra of the synthetic peptides were measured on a Jasco J-500A spectropolarimeter under nitrogen flush and calibrated with (+)-10-camphorsulfonic acid. Measurements were conducted with peptide samples in 0.1-cm path length cells at 20 °C. Spectra were obtained for each sample at wavelengths of 260 to 190–178 nm, the minimum attainable wavelength being dependent on solvent composition and ionic strength. Eight scans were collected at a scan rate of 20 nm min^{-1} with a sampling interval of 0.2 nm. Data were collected through a Jasco DP-500N data processor and then transferred to an IBM XT personal computer for analysis. Fractional helicities were calculated as $f_h = ([\theta]_{222} - [\theta]^0_{222}/[\theta]^{100}_{222}$, from the experimentally observed mean residue ellipticity $[\theta]$ at 222 nm and values for $[\theta]$ corresponding to 100% and 0% helix content at this wavelength. In a study of detergent effects on the solution conformation of melittin, Kubota and Yang (1986) selected $[\theta]^{100}_{222} = -28\,400$ deg cm^2 dmol^{-1}, with consideration to the chain-length dependence of the CD at this wavelength, and used $[\theta]^0_{222} = -2000$ deg cm^2 dmol^{-1} on the basis of observations made on a variety of denatured proteins (Wu et al., 1981). These values were used in all fractional helicity calculations.

Fluorescence Spectroscopy. Steady-state fluorescence emission spectra were obtained on a Perkin-Elmer MPF-66 fluorometer. Steady-state fluorescence anisotropy values were measured on an SLM 4800 fluorometer with excitation at 295 nm (1-nm excitation band-pass; vertically polarized excitation beam; Schott WG 345 cut-on filter in the emission path).

NMR Spectroscopy. ^{13}C and ^1H NMR spectra were obtained for each of the synthetic peptides at various concentrations in D_2O (99.5%), DMSO-d_6, or CD_3OD. Unless specifically noted, all peptide samples were buffered with 10 or 50 mM Bis-Tris, pH 6.0. A concentrated solution of buffer (0.5 M) was first prepared in H_2O, passed through a Chelex 100 column to remove residual metal ions, and then lyophilized and redissolved in an appropriate volume of D_2O which had also been passed through a Chelex 100 column prior to use. An appropriate volume of this solution was added to peptide samples dissolved in either salt-free D_2O or DMSO-d_6. DMSO-d_6 solutions contained 10% D_2O (v/v) due to addition

Table I: Mean Residue Ellipticity [θ] at 222 nm[a] and Derived Fractional Helicity (f_h) of Synthetic Melittin and Melittin Analogues in Isotropic Solvents

	MLT-W19		MLT-W17		MLT-W11		MLT-W9	
	$-[\theta]_{222}$	f_h	$-[\theta]_{222}$	f_h	$-[\theta]_{222}$	f_h	$-[\theta]_{222}$	f_h
$Na_x(PO_4)_x$								
0.017 M	4981	0.11	3423	0.05	5769	0.13	3202	0.04
0.100 M	10654	0.31	2596	0.02	5010	0.11	2529	0.02
0.200 M	16808	0.52	3356	0.05	8510	0.23	3606	0.06
CH_3OH/H_2O								
0.70 (v/v)	10837	0.31	7288	0.19	13673	0.41	9654	0.27
0.80	19875	0.63	15481	0.48	25029	0.81	17875	0.56
0.90	24625	0.80	20423	0.65	30817	1.02	23712	0.77

[a] The mean residue ellipticity at 222 nm is expressed in units of deg cm^2 dmol^{-1}. All solutions contained 20 μM peptide and 10 mM Tris, pH 7.5. Measurements were carried out at 20 °C in CD cells of 0.1-cm path length.

of the concentrated buffer in D_2O. All pH values are direct meter readings and are uncorrected for an isotope effect.

The relative solubility of the synthetic peptides in D_2O was found to be MLT-W19 ≈ MLT-W17 > MLT-W11 > MLT-W9; at room temperature, MLT-W9 was incompletely soluble at concentrations over ~2 mM. Higher concentrations (>5 mM) of MLT-W11 or MLT-W9 were attainable only at increased temperatures (30–50 °C). Upon cooling, these samples remained colorless with no observable precipitation of protein but became markedly viscous.

In the methanol titration experiments, appropriate volumes of CD_3OD were added to D_2O samples of MLT-W19, MLT-W17, or MLT-W11 to give successive D_2O to CD_3OD ratios of 90:10, 80:20, and 70:30 (v/v). Peptide concentrations decreased in proportion to the amount of CD_3OD added to the sample.

All ^{13}C NMR spectra were obtained at 75.4 MHz on a Nicolet NT-300 FT spectrometer. Approximately 5 μL of 1,4-dioxane was added to each 2.5-mL NMR sample to provide an internal ^{13}C chemical shift standard at 67.37 ppm (Shindo et al., 1978). ^{13}C NMR data were collected on the NT-300 using 12-mm tubes containing ~2.5 mL of sample solution. Broad-band noise decoupling was used to obtain proton-decoupled spectra. Proton spectra of the synthetic peptides were acquired at 300 MHz on sample volumes of ~400 μL in 5-mm tubes. ^{1}H chemical shifts were measured relative to internal sodium 2,2-dimethyl-2-silapentanesulfonate (DSS).

Results

Cytolytic Activity. That synthetic melittin retains the functional activity of the naturally occurring peptide has been noted previously (Tosteson et al., 1987). The cytolytic assay demonstrates that each of the analogues retains the ability of the native sequence (MLT-W19) to disrupt membranes. Single-exponential fits of the kinetic data from erythrocyte lysis experiments revealed the following relative cytolytic rates: MLT-W19, 0.79 ± 0.01; MLT-W17, 1.36 ± 0.01; MLT-W11, 0.67 ± 0.04; and MLT-W9, 0.15 ± 0.03 (Δo.d.) min^{-1}. Fitting the data to two exponentials did not result in a significant improvement of the fits. On the basis of this assay, the rank order of potency was found to be MLT-W17 > MLT-W19 ≈ MLT-W11 > MLT-9.

Gel Filtration. An HPLC gel filtration study of the synthetic peptides was used to investigate the effect of ionic strength on oligomer formation by MLT-W19 and the three analogues.

Retention times for the synthetic peptides in 0.1 M NaCl (low-salt) buffered solution were as follows: MLT-W19 (13.1 min); MLT-W17 (13.1 min); MLT-W11 (13.9 min); and MLT-W9 (12.9 min). In 1.2 M NaCl (high-salt) buffered solution, the following retention times were observed: MLT-W19 (11.7 min); MLT-W17 (16.2 min); MLT-W11 (17.7 min, very broad); and MLT-W9 (15.3 min). With the exception of MLT-W11 in 1.2 M NaCl, all species eluted as sharp, symmetric peaks.

Protein and small molecule standards were run for molecular volume comparisons. Retention times for the standards in 0.1 M NaCl buffered solution were as follows: serum albumin (8.4 min); hemoglobin (10.8 min); cytochrome *c* (11.7 min); lysozyme (13.0 min); and riboflavin (17.1 min). In 1.2 M NaCl, the following retention times were observed: serum albumin (8.5 min); hemoglobin (10.4 min); cytochrome *c* (11.3 min); lysozyme (12.9 min); and riboflavin (18.0 min). Each of the standards eluted as sharp, symmetric peaks in both the low- and high-salt solutions.

These results are notable for (a) approximately equal retention times for lysozyme and for the (presumably) monomeric synthetic peptides in low-salt buffer, (b) a *decreased* retention time for MLT-W19 in high-salt relative to that observed in low-salt buffer, (c) *increased* retention times for the melittin analogues in high-salt compared with those measured in low-salt buffer, and (d) essentially no NaCl-induced change in retention times for the protein standards.

CD Spectroscopy. Mean residue ellipticity at 222 nm and the corresponding fractional helicity values for the synthetic peptides are compiled in Table I. The α-helix content of MLT-W19 increases from 11% in 0.017 M sodium phosphate to 52% in 0.2 M sodium phosphate. Measurements performed at similar peptide concentrations but in the presence of 0.8 M sodium phosphate suggest a maximum attainable helicity of ~75% for MLT-W19 (Fisher and Prendergast, unpublished data). Of the three melittin analogues, only MLT-W11 reveals an appreciable salt-induced increase in helix content (13% → 23%). MLT-W17 and MLT-W9 demonstrate ≤6% α-helix content at phosphate concentrations up to 0.2 M.

The methanol titration data obtained for MLT-W19 agree almost exactly with the data of Chandani and Balasubramanian (1986) in showing a nearly linear increase in molar ellipticity at 222 nm with methanol content. In 90% methanol, MLT-W19 appears to be about 80% helical (21 of 26 residues). Notably, the α-helix content of MLT-W11 is predicted to be 102% by the method of analysis we chose (Kubota & Yang, 1986). Although all of the analogues retain appreciable helix-forming potential, MLT-W17 and MLT-W9 appear to be somewhat less efficient in this regard than MLT-W19 or MLT-W11.

Fluorescence Spectroscopy. The response of the fluorescence emission maximum (λ_{max}) and the fluorescence steady-state anisotropy ($\bar{r}$) to titration with NaCl is illustrated in Figure 2. Of the synthetic peptides, only MLT-W19 exhibits a pronounced salt-induced blue shift (351 → 337 nm).

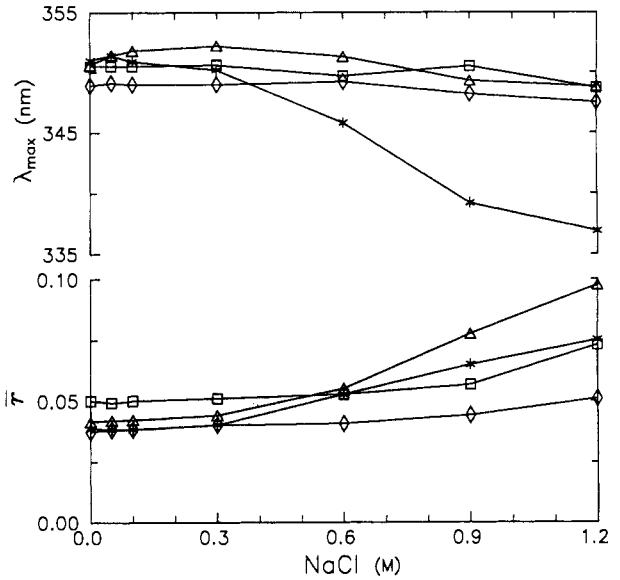

FIGURE 2: Fluorescence emission maxima (λ_{max}) and steady-state fluorescence anisotropy ($\bar{r}$) values of MLT-W19 and analogues as a function of NaCl concentration in water. MLT-W19 (*); MLT-W17 (◊); MLT-W11 (△); MLT-W9 (□). All solutions contained 20 μM peptide and 10 mM Tris, pH 7.5. All measurements were carried out at 20 °C. Steady-state anisotropy values were measured at an excitation wavelength of 295 nm.

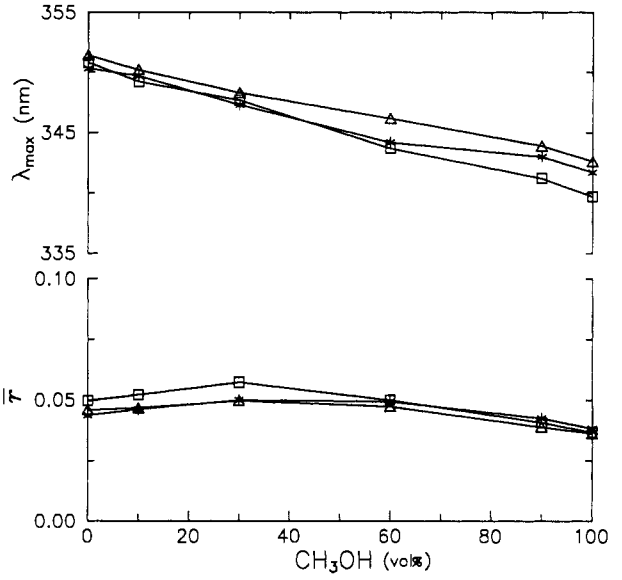

FIGURE 3: Fluorescence emission maxima (λ_{max}) and steady-state fluorescence anisotropy ($\bar{r}$) for MLT-W19 and analogues as a function of methanol content in water. MLT-W19 (*); MLT-W11 (△); MLT-W9 (□). All solutions contained 20 μM peptide and 10 mM Tris, pH 7.5. All measurements were carried out at 20 °C. Steady-state anisotropy values were measured at an excitation wavelength of 295 nm. Data were not collected for MLT-W17.

This phenomenon has been correlated with the structural transition from monomer to tetramer in the naturally occurring peptide (Talbot et al., 1979). Although steady-state anisotropy values for each of the synthetic peptides increase with NaCl content, MLT-W19 does *not* show the greatest increment in spite of tetramer formation. Instead, MLT-W11 exhibits the largest value, while MLT-W9 demonstrates only a small increment in the presence of 1.2 M NaCl. The lower $\bar{r}$ value observed for MLT-W19 (0.039) agrees almost exactly with that observed by others for naturally occurring melittin, while the upper value (0.072) is somewhat less than a value of 0.10 recorded for synthetic melittin at still higher salt concentrations (Fisher and Prendergast, unpublished data).[4]

In water/methanol solutions, there is a nearly identical and approximately linear decrease in λ_{max} with increasing methanol content for each of the peptides (Figure 3). Free tryptophan shows comparable behavior under similar conditions (data not shown). Figure 3 also shows that steady-state fluorescence anisotropy values for the synthetic peptides fall slightly with increasing methanol content and approach virtually identical values in 90% methanol.

NMR Spectroscopy. ^{13}C and ^1H NMR spectra were obtained for the synthetic peptides in D_2O, D_2O/NaCl, D_2O/CD_3OD, and DMSO-d_6/D_2O solutions. Chemical shift values and ^{13}C line widths for Trp δ_1-carbon and Gly-12 α-carbon resonances of the peptides are compiled in Table II.

(1) Aqueous Solutions. The aromatic region of the ^1H NMR spectra of MLT-W19 and MLT-W17 are shown in Figure 4. With the exception of the H-$^{13}C\delta_1$ resonance, these spectra show the usual doublet or triplet resonances for each of the indole ring protons. The $^{13}C\delta_1$ proton of MLT-W19 (Figure 4a) appears as a widely split doublet centered at 7.25 ppm with an upfield peak at 6.95 ppm and a downfield partner at 7.55 ppm. The indole proton resonances of MLT-W11 and MLT-W9 (data not shown) coincided with those observed for MLT-W19. Interestingly, the downfield peak of the H-$^{13}C\delta_1$ doublet of MLT-W17 (Figure 4b) is superimposed upon an upfield-shifted H-Cζ_2 doublet at 7.56 ppm. Contrasted with the similarity in ^1H NMR spectra obtained for the other peptides under like conditions, the shifted Trp-17 H-Cζ_2 resonance of MLT-W17 monomer may indicate that the indole moiety adopts some distinct or preferred orientation in this peptide. Unfortunately, it was not possible to readily identify the ^{13}C-coupled Gly-12 proton resonances in the aliphatic region of the ^1H NMR spectra of the synthetic peptides.

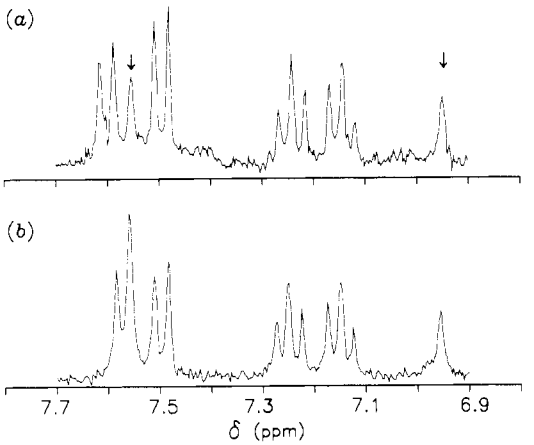

FIGURE 4: Aromatic region of ^1H NMR spectra obtained for monomeric MLT-W19 and MLT-W17 at 300.1 MHz. In (a), the Trp-19 H-$^{13}C\delta_1$ doublet (arrows) is centered at 7.25 ppm (^1J = 181.6 Hz). Spectra obtained for MLT-W11 and MLT-W9 were very similar. In (b), an upfield-shifted H-Cζ_2 doublet now overlies the upfield peak of the Trp-17 H-$^{13}C\delta_1$ doublet centered at 7.25 ppm (^1J = 181.6 Hz). Both spectra were obtained at peptide concentrations of 0.5 mM in D_2O, pH 4.1, 20 °C. Chemical shifts are given relative to internal DSS.

The ^{13}C NMR spectra of MLT-W19, MLT-W17, and MLT-W11 at concentrations of ~1 mM in D_2O were very similar—Trp Cδ_1 and Gly-12 Cα peaks occurred at 124.9–125.3 ppm and 43.0–43.1 ppm, respectively. Comparable ^1J values were measured for the $^{13}C\delta_1$ doublet (180–181 Hz) and $^{13}C\alpha$ triplet (141–142 Hz) resonances of MLT-W19, MLT-W17, and MLT-W11 from proton-coupled ^{13}C spectra.

[4] $\bar{r}$(295 nm) = 0.100 for nonisotopically labeled synthetic melittin in 2 M NaCl at 20 °C.

Table II: Chemical Shifts and Line Widths Determined from ^{13}C NMR Spectra Obtained at 75.4 MHz for MLT-W19 and Analogues in Isotropic Solvents[a]

solvent	sample concn (mM)	Trp $^{13}C\delta_1$ δ (ppm)[b]	Trp $^{13}C\delta_1$ $\Delta\nu$ (Hz)[c]	Gly-12 $^{13}C\alpha$ δ (ppm)	Gly-12 $^{13}C\alpha$ $\Delta\nu$ (Hz)	dδ (ppm)[d]
			MLT-W19			
D_2O	5.08	125.09	17.3	44.79	21.1	80.30
	1.11	125.06	6.4	42.99	10.3	82.07
NaCl						
0.2 M	1.05	125.43	34.7	44.55/43.12	27.8/–	80.88/82.31
0.5 M	0.97	125.53	27.4	44.43/43.14	30.3/8.7	81.10/82.39
1.0 M	0.83	124.64	5.9	44.46/43.24	15.0/–	80.18/81.40
CD_3OD/D_2O						
0.10 (v/v)	4.57	124.91	19.8	44.71	28.6	80.20
0.20 (v/v)	4.06	124.72	23.0	44.60	33.1	80.12
0.30 (v/v)	3.56	124.54		44.27		80.27
0.10 (v/v)	1.00	124.97	11.3	43.04	17.0	81.93
0.20 (v/v)	0.89	124.85	11.0	43.20	22.9	81.65
0.30 (v/v)	0.78	124.64	8.2	43.10	11.1	81.54
DMSO-d_6/D_2O						
0.90 (v/v)	5.55	124.42	13.4	42.78	14.4	81.64
			MLT-W17			
D_2O	5.74	124.92	14.8	43.29	18.9	81.63
	1.15	124.93	8.1	43.03	7.8	81.90
NaCl						
0.2 M	1.09	124.94	10.1	43.12	11.3	81.82
0.5 M	1.00	124.94	14.4	43.55	22.7	81.39
1.0 M	0.86	124.90	32.1	44.11	19.2	80.79
CD_3OD						
0.10 (v/v)	1.04	124.75	9.6	43.01	9.9	81.74
0.20 (v/v)	0.92	124.51	7.7	42.98	8.9	81.53
0.30 (v/v)	0.81	124.17	9.3	43.03	8.5	81.14
DMSO-d_6						
0.90 (v/v)	5.83	124.31	13.9	42.77	15.9	81.54
			MLT-W11			
D_2O	6.45	125.55		44.63/43.35	–/–	80.92/82.20
	1.29	125.18	8.1	43.04	18.7	82.14
NaCl						
0.2 M	1.23	125.53	25.8	44.27/43.44		81.26/82.09
CD_3OD						
0.10 (v/v)	1.16	125.10	14.4	43.12	26.2	81.98
0.20 (v/v)	1.03	124.91	16.9	43.16	32.5	81.75
0.30 (v/v)	0.90	124.64	11.2	43.02	23.1	81.62
DMSO-d_6						
0.90 (v/v)	5.35	124.54	17.3	42.84	22.8	81.70
			MLT-W9			
D_2O	0.81	125.26		43.09		82.17
DMSO-d_6						
0.90 (v/v)	6.13	124.62	14.0	42.90	21.4	81.72

[a] Concentrated samples (>5 mM) in D_2O or 90% DMSO-d_6 were buffered with 50 mM Bis-Tris, pH 6.0. All other samples in D_2O were buffered with 10 mM Bis-Tris, pH 6.0. [b] Chemical shift values are given relative to tetramethylsilane (TMS) and are referenced to internal 1,4-dioxane at 67.37 ppm (Shindo et al., 1978). ^{13}C chemical shift values are typically accurate to ±0.05 ppm. [c] Line widths are expressed as full width at half-maximum signal intensity. Line widths could not be reliably measured for extremely broad peaks (>100 Hz) and for those resonances having very low signal to noise. [d] dδ values are calculated as the difference $\delta_{Trp} - \delta_{Gly}$.

The proton-coupled ^{13}C NMR spectrum of a more concentrated sample of MLT-W19 (5.08 mM), shown in Figure 5, was remarkable for a pronounced downfield shift of the Gly-12 α-carbon resonance to 44.8 ppm, while the chemical shift of the Trp-19 $C\delta_1$ peak showed no change (see Table II).

Chemical shift values in Table II are also given in terms in $d\delta = \delta_{Trp} - \delta_{Gly}$, i.e., the difference in the Trp $^{13}C\delta_1$ and Gly-12 Cα chemical shifts for a given sample. This parameter was found to be sensitive to helix formation, yet relatively free from solvent effects (see below). The peptide concentration-dependent change in dδ of 1.77 ppm (=82.07–80.30) suggests that the magnetic environment of the Gly-12 backbone α-carbon of MLT-W19 is quite sensitive to the conformation and/or aggregation state of the peptide.

The assignment of the upfield and downfield Gly-12 Cα peaks to monomeric (random coil) and tetrameric (α-helical) MLT-W19, respectively, was confirmed by investigating the dynamics of the monomer $\rightleftharpoons$ tetramer equilibrium by titrating the 1.11 mM peptide sample with NaCl. Proton-decoupled ^{13}C NMR spectra of MLT-W19 obtained in 0.0, 0.2, 0.5, and 1 M NaCl are shown in Figure 6. In each of the NaCl-containing samples, the Gly-12 α-carbon resonance is clearly split into two peaks centered at ~43.1 and ~44.5 ppm. These two peaks coincide, respectively, with the position of the single Gly-12 Cα resonance observed in monomer- and tetramer-predominant samples of MLT-W19 in salt-free D_2O. The simultaneous presence of both Cα signals in NaCl-containing samples indicates that monomer and tetramer are in slow exchange ($\leq$120 s^{-1}). In contrast, the nondoubled and unshifted Trp $C\delta_1$ resonance implies that the magnetic environment of the pyrrole portion of the Trp side chain is not appreciably different in the monomer and tetramer. Further, the existence of single Gly-12 Cα and Trp-19 $C\delta_1$ peaks in tetramer-predominant samples of MLT-W19 indicates that the magnetic environment of the respective ^{13}C labels of each peptide chain is essentially the same—a result that is taken

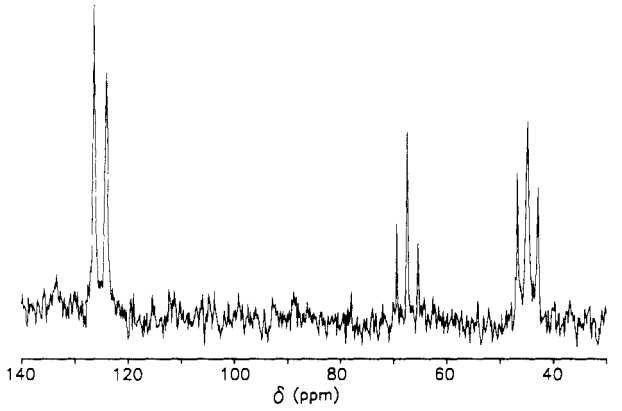

FIGURE 5: Proton-coupled ^{13}C NMR spectrum of tetrameric MLT-W19 obtained at 75.4 MHz in salt-free D_2O. The H_2-$^{13}C\alpha$ of Gly-12 appears as a triplet centered at 44.79 ppm (^1J = 141.5 Hz) and the H-$^{13}C\delta_1$ of Trp-19 as a doublet centered at 125.1 ppm (^1J = 180.2 Hz). The 1,4-dioxane reference appears as a triplet at 67.37 ppm. This spectrum was obtained at a peptide concentration of 5.08 mM in D_2O, pH 6.0, 20 °C.

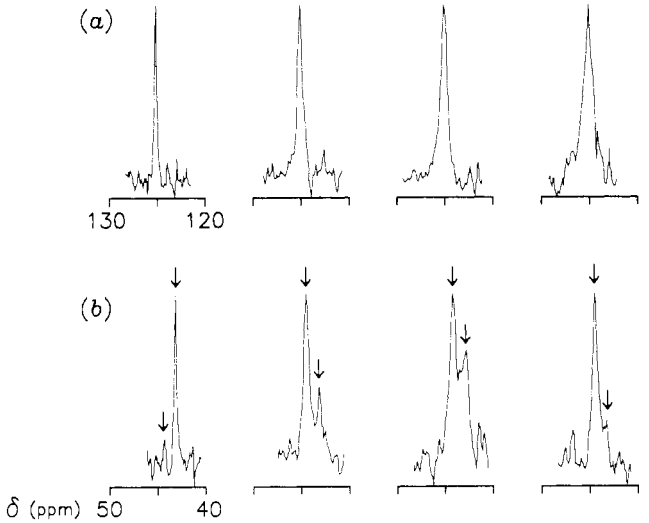

FIGURE 6: Peptide ^{13}C resonances from proton-decoupled ^{13}C NMR spectra of MLT-W19 obtained at 75.4 MHz in D_2O. The Trp-19 $^{13}C\delta_1$ and Gly-12 $^{13}C\alpha$ resonances are shown in panels a and b, respectively. Spectra were obtained, from left to right, at peptide concentrations of 1.11, 1.00, 0.89, and 0.78 mM in the presence of 0.0, 0.2, 0.5, and 1.0 M NaCl, respectively. For clarity, peak heights are normalized. Tic marks along the abscissae mark chemical shift intervals of 5 ppm. In panel a, the chemical shift of the Trp-19 δ_1-carbon peak does not change with salt concentration, although its line width increases. In panel b, the doubled α-carbon resonance shows peaks at ~44.5 and ~43.1 ppm corresponding to the tetrameric (α-helical) and monomeric (random coil) forms of melittin, respectively. The dilutional decrease in peptide concentration apparently offsets the effect of increased ionic strength, resulting in a relative increase monomer peak area for the sample containing 0.5 M NaCl. All samples were buffered with 10 mM Bis-Tris, pH 6.0, and obtained at a probe temperature of 20 °C.

to reflect the symmetry of the oligomer. A similar observation was made by Brown et al. (1980) with regard to the proton resonances of melittin tetramer.

As observed for MLT-W19, the Trp $C\delta_1$ resonance did not shift upon titration of MLT-W17 and MLT-W11 with NaCl (Table II). The Gly-12 $C\alpha$ resonance, however, showed a marked response to NaCl or increased peptide concentration and exhibited distinct behavior in each of these analogues. A downfield shift of 0.26 ppm was observed for the Gly-12 $C\alpha$ in a concentrated sample of MLT-W17 (5.74 mM) relative to that observed in a more dilute sample (1.15 mM). ^{13}C NMR spectra of MLT-W17 in 0.2, 0.5, and 1.0 M NaCl, respectively, showed the gradual downfield shift of an increasingly broad Gly-12 $C\alpha$ peak. This behavior suggested partial helix formation coincident with presumably nonspecific peptide aggregation. Discrete, titratable monomer and oligomer resonances were not observed as with MLT-W19.

The ^{13}C NMR spectrum of a concentrated sample of MLT-W11 (6.45 mM) in D_2O showed a very broad Trp-11 $C\delta_1$ peak (~100 Hz) at 125.6 ppm. The Gly-12 $C\alpha$ peak was extremely broad (~400 Hz) and appeared to contain two peaks, the larger of which was centered at 44.6 ppm, the smaller at 43.4 ppm. As with MLT-W17, the broad lines again suggested extensive nonspecific, higher order peptide aggregation. The occurrence of the more prominent Gly-12 $C\alpha$ resonance at a value close to that observed for tetrameric MLT-W19 (44.8 ppm) suggested that MLT-W11 also becomes predominantly helical under these conditions. In contrast, the ^{13}C NMR spectrum of a less concentrated sample of MLT-W11 (1.29 mM) showed ^{13}C resonances and line widths comparable with those recorded for monomeric MLT-W19 and MLT-W17 in salt-free D_2O—no downfield shift of the Gly-12 $C\alpha$ peak was observed. However, on addition of 0.2 M NaCl, the $C\alpha$ resonance was split into two broad overlapping peaks centered at 43.4 and 44.3 ppm, respectively (Table II); in 0.5 M NaCl, a spectrum could not be obtained, presumably due to extensive line broadening. Again, salt-induced helix formation accompanied by higher order peptide self-association was suggested by the downfield shift and broadening of the MLT-W11 $C\alpha$ peak.

At a concentration of 1.63 mM in D_2O, MLT-W9 did not yield a ^{13}C NMR spectrum, presumably due to aggregation in the gel-like sample. However, a spectrum was obtained for the 2-fold-diluted sample in D_2O, revealing very broad resonances centered at 125.4 and 43.1 ppm for the Trp-9, $C\delta_1$ and Gly-12 $C\alpha$ labels, respectively. In contrast to MLT-W19, MLT-W17, and MLT-W11, the behavior of the Gly-12 $C\alpha$ chemical shift suggested that MLT-W9 does *not* become helical despite extensive self-association at this concentration in D_2O.

(*2*) *Water/Methanol Solutions.* That methanol induces helix formation in MLT-W19 and analogues is evident from the CD data presented above. Titration of D_2O samples of MLT-W19, MLT-W17, and MLT-W9 with methanol (CD_3OD) was carried out to identify changes in ^{13}C NMR parameters that accompany methanol-induced helix formation. The effect of methanol on MLT-W19 tetramer stability was also investigated. Chemical shifts and line widths for Trp $C\delta_1$ and Gly-12 $C\alpha$ peaks are compiled in Table II for samples of MLT-W19, MLT-W17, and MLT-W11 containing 10–30% CD_3OD.

The Trp $C\delta_1$ resonance of each of the peptides exhibited a progressive upfield shift with increasing methanol concentration. The Gly-12 $C\alpha$ resonance of MLT-W19 and MLT-W11 initially shifted downfield in 10% and 20% CD_3OD but then showed a small upfield shift in 30% CD_3OD; much smaller Gly-12 $C\alpha$ shifts ($\leq$0.05 ppm) were observed for MLT-W17. Contrasted with the behavior of the Gly-12 $C\alpha$ resonance, the *upfield* shift of the Trp $C\delta_1$ peak suggested the possibility of a uniform solvent-dependent displacement of chemical shifts which could offset in part, or entirely, a downfield shift of the Gly-12 $C\alpha$ resonance due to partial α-helix formation in the D_2O/CD_3OD mixtures. The extent of helix formation per se can be isolated by examining $d\delta$ values (see Table II). The Gly-12 α-carbon resonance exhibits a small but consistent downfield shift in all of the peptides as the methanol content is raised (~0.2 ppm/10 vol % added methanol). This trend

predicts a total downfield shift of ~2.0 ppm in 100% methanol, which is comparable to the 1.8 ppm shift noted for this resonance in tetrameric melittin, where 92% of residues are contained in α-helical secondary structure.[5] The case for partial methanol-induced helix formation in the monomeric peptides is also supported by the observation that titration of MLT-W19 *tetramer* with CD_3OD results in an upfield shift of *both* the Trp Cδ_1 and Gly-12 Cα peaks equal in magnitude to the shift noted for the Trp Cδ_1 resonance *only* of the monomeric peptides.

(*3*) *Dimethyl Sulfoxide/Water Solutions.* In order to characterize the synthetic peptides under conditions that disrupt both hydrophobic and hydrogen-bonding interactions, ^{13}C NMR spectra were obtained for these species in 90% DMSO-d_6/10% D_2O. In this solvent system, linear peptides can reasonably by assumed to be devoid of stable secondary structure. The unordered or random coil state serves as a useful reference state for evaluation of data collected for MLT-W19 and analogues in water or other solvents that promote peptide secondary structure.

Concentrated solutions (5–10 mM) of MLT-W19 and analogues in this solvent system showed sharp resonances suggestive of relatively rapid and unhindered motion of the peptide ^{13}C labels. In contrast to spectra obtained in water or water/methanol mixtures, ^{13}C NMR spectra of the synthetic peptides in 90% DMSO-d_6 were all very similar. Chemical shift and line-width data are summarized in Table II.

As in D_2O, ^{13}C chemical shifts are given relative to internal 1,4-dioxane even though the reference value of 67.37 ppm (Shindo et al., 1978) is probably not accurate in 90% DMSO-d_6. As in the water/methanol mixtures, a uniform upfield shift of the Trp and Gly-12 ^{13}C resonances is indicative of a general solvent-dependent displacement of chemical shifts. Notably, however, the downfield shift of the Gly-12 Cα resonance that characterizes helix formation in water or water/methanol mixtures does not occur in DMSO. Although dδ values in DMSO might suggest partial helix formation by comparison with those observed in water/methanol mixtures, there is essentially no difference between the observed dδ values (81.5–81.7 ppm) and dδ calculated from the appropriate resonances of the free amino acids dissolved in DMSO (81.4 ppm) (Grathwohl & Wüthrich, 1974). This result is consistent with the presumed unstructured state of the peptides in this solvent.

Finally, it is worth noting that the ^{13}C NMR spectrum of MLT-W9 was essentially identical with those of MLT-W19, MLT-W17, and MLT-W11 in this solvent. This observation reinforces the presumption that aggregation of MLT-W9 is responsible for the failure to observe resonances for this analogue at concentrations above ~1 mM in aqueous media.

Discussion

The synthetic peptides characterized in this work were designed to investigate associations between membranolytic activity, amphiphilic helix formation, and peptide oligomerization. As a paradigm for such studies, melittin is an excellent choice because it is known to be a potent cytolysin (Sessa et al., 1969), to become α-helical in helicogenic solvents (Lavialle et al., 1982; Chandani & Balasubramanian, 1986), and to become helical and tetrameric under conditions of high ionic strength and/or pH (Talbot et al., 1979). Not surprisingly, the spectroscopic and functional properties of synthetic isotopically labeled melittin proved indistinguishable from those of the naturally occurring product.

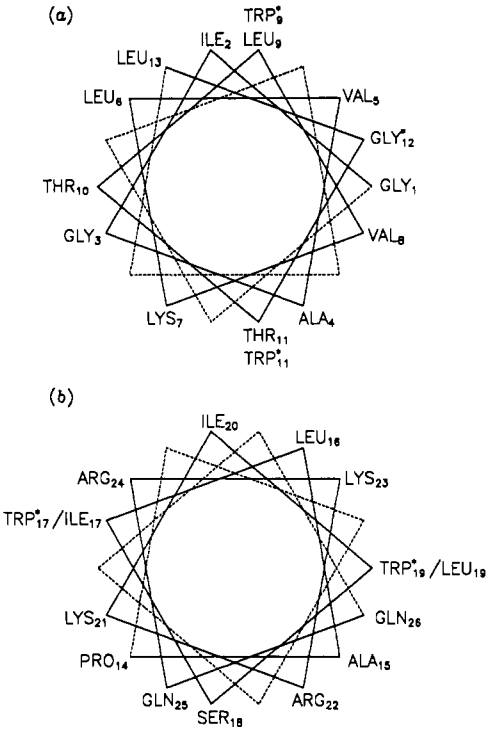

FIGURE 7: Helical wheel diagrams of MLT-W19 and analogues. Residues 1–13 and 14–26 are shown in panels a and b, respectively. The innermost residues correspond to the sequence of MLT-W19; amino acid substitutions made in the analogues are shown peripherally. The Trp-9 residue of MLT-W9 and Trp-11 of MLT-W11 are positioned on opposite faces of the N-terminal amphiphilic helix (a), while Trp-17 of MLT-W17 and Trp-19 of MLT-W19 are located on opposite faces of the C-terminal amphiphilic helix (b). ^{13}C-Labeled residues are starred. Linear sequences of the synthetic peptides are given in Figure 1.

HPLC and spectroscopic data obtained for relatively dilute solutions (<~1 mM) of melittin and three analogues in water showed that the peptides are essentially unstructured under these conditions. HPLC gel permeation retention times for the peptide monomers in dilute aqueous buffer were not only very similar but also shorter than would be expected on the basis of molecular weight alone—a result consistent with an "extended" conformation for the random coil peptides. Moreover, ^{13}C NMR spectra of the peptides in DMSO/D_2O were essentially identical in this solvent which discourages both hydrophobic and hydrogen-bonding interactions. These results provide a "base line" for interpretation of HPLC and spectroscopic data obtained for these peptides in other solvents.

The melittin analogues were designed by using the template provided by the native sequence and differ from the latter only in the substitution of Leu-19 for Trp-19 and in the replacement of Leu-17, Thr-11, or Leu-9 with [^{13}Cδ_1]Trp, respectively. The helical wheel diagrams (Schiffer & Edmundson, 1967) of Figure 7 show the relative position of the single Trp residue in melittin and the analogues. The Trp side chain of MLT-W11 is apparently in the most polar environment with respect to neighboring side chains, while that of MLT-W9 lies amid nonpolar residues. The Trp side chains of MLT-W19 and MLT-W17 are situated approximately at the boundary between polar and nonpolar residues, but on opposite faces of the amphiphilic helix. Fluorescence and NMR studies of these

[5] Subsequently, we have obtained Gly-12 ^{13}Cα chemical shift data for MLT-W19 monomer in D_2O–CD_3OD solutions using 1,4-dioxane in D_2O as an *external* reference. As postulated, we observe a progressive downfield shift of the Gly-12 ^{13}Cα resonance from 43.0 ppm in 100% D_2O to 44.6 ppm in 100% CD_3OD, while the Trp-19 ^{13}Cδ_1 resonance shows a small upfield shift from 125.0 to 124.7 ppm.

peptides thus probe the environment of a single ^{13}C-labeled Trp side chain at distinct locations along the melittin α-helix.

The CD data show that the position of the Trp residue influences the extent of helix formed by the peptides in water/methanol mixtures (see Table I). The molecular basis for such differences is not clear. The variation in fractional helix content is unlikely to be due to oligomer formation in the water/methanol mixtures given (a) the minimal differences in the Trp fluorescence anisotropy profiles and the absence of an increase in anisotropy values with increasing methanol content and (b) the lack of NMR evidence for aggregation. It is important to note that the CD results reported here agree well with those of Chandani and Balasubramanian (1986), with the 2-D ^1H NMR study of Bazzo et al. (1988), and with inferences made from UV resonance Raman measurements (Hildebrandt et al., 1989) which find that melittin is helical along nearly its entire length in neat methanol. The ^{13}C NMR data also support partial α-helix formation by the peptides in D_2O containing 10–30% methanol. Given these results, it appears that helix formation and helix stability in each peptide are influenced by interactions among side chains. Lastly, despite the presence of the Pro-14 residue, the high helical content of all of the peptides in 90% methanol suggests that other factors can overcome the inherent helix-destabilizing influence of this residue (Barlow & Thornton, 1988).

A comparison of CD, fluorescence, and NMR spectra obtained for melittin and analogues apparently allows one to discriminate between helix formation per se and peptide self-association. Melittin tetramer is known from its crystal structure (Terwilliger & Eisenberg, 1982a,b) to be composed of α-helical peptide monomers. In the crystalline tetramer, the Trp-19 side chains become partially buried in the protein matrix. These structural features are corroborated by CD and fluorescence measurements on the soluble tetramer. It is interesting that ^{13}C NMR studies indicate that the chemical shift of the indole ring $^{13}C\delta_1$ is not perturbed by tetramer formation. Computer graphics examination of the tetramer crystal structure shows that the symmetry-related Trp-19 $C\delta_1$ atoms remain essentially fully solvent accessible, while most of the phenyl portion of the indole ring is tucked into a relatively solvent-inaccessible pocket.

In contrast to the behavior of the Trp-19 $^{13}C\delta_1$ resonance, the Gly-12 α-carbon resonance moves downfield by $\sim$1.8 ppm upon tetramer formation. Since the Gly-12 $^{13}C\alpha$ label is positioned near the polar–apolar interface of the melittin amphiphilic helix (see Figure 7), it was initially unclear whether the downfield shift of this resonance was primarily due to intermolecular interactions (i.e., "internalization" of the Gly-12 $C\alpha$ with concomitant sequestration away from solvent) or to intramolecular interactions (i.e., hydrogen bonding attending helix formation). ^{13}C NMR spectra of the synthetic peptides in D_2O/CD_3OD solutions give evidence favoring the latter interpretation. In support of this, we note that doubling of a peptide α-carbon resonance has been observed for α-helical poly(L-glutamic acid) (Lader et al., 1977). Specifically, these authors found that a downfield $C\alpha$ peak at $\sim$56.7 ppm becomes more prominent as the solution pH is lowered and helix content increases. Concomitantly, an upfield $C\alpha$ peak at $\sim$54.5 ppm diminishes. The difference in the chemical shift values is 2.2 ppm. At neutral pH, with the peptide in a random coil state, only the upfield peak is observed. It appears that the helix–coil transition of melittin and the melittin analogues presents a similar phenomenon; hence, we ascribe the observed Gly-12 $C\alpha$ shift to monomeric helix formation rather than peptide oligomerization.

Despite the fact that all of the melittin analogues retain the capacity to become α-helical, the ability to form a tetramer appears to be unique to melittin itself. The HPLC results and spectroscopic properties of the peptides indicate that although the melittin analogues show a propensity for nonspecific aggregation at high peptide or salt concentrations, there is no evidence for formation of a discrete tetramer except by MLT-W19. The similarity of retention times for MLT-W19 and cytochrome *c* in high ionic strength solution is in keeping with melittin's presumed tetrameric state under these conditions. In contrast, the much longer retention times for the melittin analogues in high-salt buffer are not consistent with oligomer formation. Similarly, spectroscopic data fail to support formation of discrete oligomeric species by any of the melittin analogues at high ionic strength. Although comparable steady-state fluorescence anisotropy values for MLT-W9, MLT-W11, and MLT-W19 tetramer in high ionic strength solutions might be attributed to formation of discrete oligomers by each of these peptides, nonspecific peptide aggregation of the melittin analogues is a more plausible interpretation in light of the NMR evidence presented above.

The apparent failure of the analogues to form melittin-like tetramers prompted a close examination of the melittin crystal structure. It appears that specific side-chain interactions, including a careful packing of the indole moieties into a pocket formed by several apolar residues, may stabilize the protein. While the amino acid substitutions in MLT-W17 and MLT-W9 are conservative in the sense that these analogues preserve the amino acid composition of the native sequence, the substitutions are only semiconservative in terms of the hydrophobicity [cf. Nozaki and Tanford (1971) and Janin (1979)] and steric bulk of the respective side chains. The Thr-11 $\rightarrow$ Trp-11 substitution of MLT-W11 is obviously nonconservative. Finally, the leucine side chain at position 19 may not substitute well sterically for the displaced tryptophan side chain in the analogues. In addition, the displaced Trp side chain might disrupt side-chain packing at interhelix interaction sites, especially in MLT-W9.

The importance of the Trp residue to oligomer stabilization might be inferred from the relative solubility of the analogues in aqueous solutions. The tendency of the peptides to aggregate in aqueous media was found to be MLT-W9 > MLT-W11 $\gg$ MLT-W17 $\approx$ MLT-W19. A plausible explanation for this pattern is that displacement of the Trp side chain away from the peptide C-terminus permits the Trp residue to participate in intermolecular hydrophobic interactions which would otherwise be discouraged by repulsive electrostatic interactions between positively charged side chains near the C-terminus of melittin.

Overall, we are able to draw the following conclusions. First, the spectroscopic results highlight the importance of solvent in determining the extent of helical secondary structure and self-association by these amphiphilic peptides. Second, in aqueous environments, melittin helix formation and tetramer assembly appear to be concurrent and mutually dependent processes. Since the analogues do retain the ability to form amphiphilic helices, it can be inferred that they violate protein packing constraints which otherwise allow or facilitate tetramer formation. Given the similarity of the analogues to melittin, a more precise delineation of structural parameters important for assembly of melittin tetramer should be possible. Third, the analogues demonstrate that the ability to form a soluble tetramer is certainly *not* a prerequisite for cytolysis. Fourth, helix-forming potential, while probably important for cytolytic activity, does not seem to be precisely correlated with this

ability. In isotropic solutions, stability of monomeric helices may be determined by specific side-chain interactions rather than the overall amphiphilicity of the peptide helix. Finally, repulsive electrostatic interactions between charged amino acid side chains near the melittin C-terminus appear to be important in discouraging intermolecular hydrophobic contacts involving the Trp-19 side chain and may explain the relative solubility of the melittin analogues.

In sum, the functional and spectral characterization of the ^{13}C-labeled synthetic peptides in isotropic solvents facilitates a structure-based interpretation of Trp side chain and peptide backbone dynamics, which we present in the following article (Weaver et al., 1989).

Acknowledgments

We thank the Physics Department of Indiana University–Purdue University at Indianapolis (IUPUI) for use of their NMR facilities. This paper is taken in part from the doctoral thesis of one of us (A.J.W.).

References

Barlow, D. J., & Thornton, J. M. (1988) *J. Mol. Biol. 201*, 601–619.

Bazzo, R., Tappin, M. J., Pastore, A., Harvey, T. S., Carver, J. A., & Campbell, I. D. (1988) *Eur. J. Biochem. 173*, 139–146.

Branchini, B. R., Prendergast, F. G., Spencer, G. A., Hagdahl, J. D., Ray, B. D., & Kemple, M. D. (1987) *J. Labelled Compds. Radiopharm. 24*, 637–643.

Brown, L. R., Lauterwein, J., & Wüthrich, K. (1980) *Biochim. Biophys. Acta 622*, 231–244.

Chandani, B., & Balasubramanian, D. (1986) *Biopolymers 25*, 1259–1272.

Faucon, J. F., Dufourcq, J., & Lussan, C. (1979) *FEBS Lett. 102*, 187–190.

Grathwohl, C., & Wüthrich, K. (1974) *J. Magn. Reson. 13*, 217–255.

Hildebrandt, P. G., Copeland, R. A., Perno, J. G., Spiro, T. G., & Prendergast, F. G. (1989) *Biochemistry* (submitted for publication).

Janin, J. (1979) *Nature 227*, 491–492.

Knöppel, E., Eisenberg, D., & Wickner, W. (1979) *Biochemistry 18*, 4177–4181.

Kubota, S., & Yang, J. T. (1986) *Biopolymers 25*, 1493–1504.

Lader, H. J., Komoroski, R. A., & Mandelkern, L. (1977) *Biopolymers 16*, 895–905.

Lauterwein, J., Brown, L. R., & Wüthrich, K. (1980) *Biochim. Biophys. Acta 622*, 219–230.

Lavialle, F., Adams, R. G., & Levin, I. W. (1982) *Biochemistry 21*, 2305–2312.

Moroder, L., Hallett, A., Wünsch, E., Keller, O., & Wersin, G. (1976) *Hoppe-Seyler's Z. Physiol. Chem. 357*, 1651–1653.

Nozaki, Y., & Tanford, C. (1971) *J. Biol. Chem. 246*, 2211–2217.

Quay, S. C., & Condie, C. C. (1983) *Biochemistry 22*, 695–700.

Schiffer, M., & Edmundson, A. B. (1967) *Biophys. J. 7*, 121–135.

Schröder, E., Lübke, K., Lehrmann, M., & Beetz, I. (1971) *Experientia 27*, 764–765.

Sessa, G., Freer, J. H., Colacicco, G., & Weisman, G. (1969) *J. Biol. Chem. 244*, 3575–3582.

Shindo, H., Egan, W., & Cohen, J. S. (1978) *J. Biol. Chem. 253*, 6751–6755.

Talbot, J. C., Dufourcq, J., de Bony, J., Faucon, J. F., & Lussan, C. (1979) *FEBS Lett. 102*, 191–193.

Tatham, A. S., Hider, R. C., & Drake, A. F. (1983) *Biochem. J. 211*, 683–686.

Terwilliger, T. C., & Eisenberg, D. (1982a) *J. Biol. Chem. 257*, 6010–6015.

Terwilliger, T. C., & Eisenberg, D. (1982b) *J. Biol. Chem. 257*, 6016–6022.

Tosteson, M. T., Levy, J. J., Caporale, L. M., Rosenblatt, M., & Tosteson, D. C. (1987) *Biochemistry 26*, 6627–6631.

Vogel, H. (1981) *FEBS Lett. 134*, 37–42.

Weaver, A. J., Kemple, M. D., & Prendergast, F. G. (1988) *Biophys. J. 54*, 1–15.

Weaver, A. J., Kemple, M. D., & Prendergast, F. G. (1989) *Biochemistry* (following paper in this issue).

Wu, C. S. C., Ikeda, K., & Yang, J. T. (1981) *Biochemistry 20*, 566–570.